Supporting Information

Mechanism and kinetics of Propane dehydrogenation and cracking over Ga/H-MFI prepared via vapor-phase exchange of H-MFI with $GaCl_3$

Neelay M. Phadke[1], Erum Mansoor[1], Matthieu Bondil[2], Martin Head-Gordon[3], Alexis T. Bell[1*]

[1]Department of Chemical and Biomolecular Engineering, University of California, Berkeley, CA 94720

[2]Ecole Polytechnique Federale de Lausanne, Lausanne, CH-1015

[3]Department of Chemistry, University of California, Berkeley, CA 94720

‡ Contributed equally to this work.

*To whom correspondence should be addressed: alexbell@berkeley.edu

Text S1.

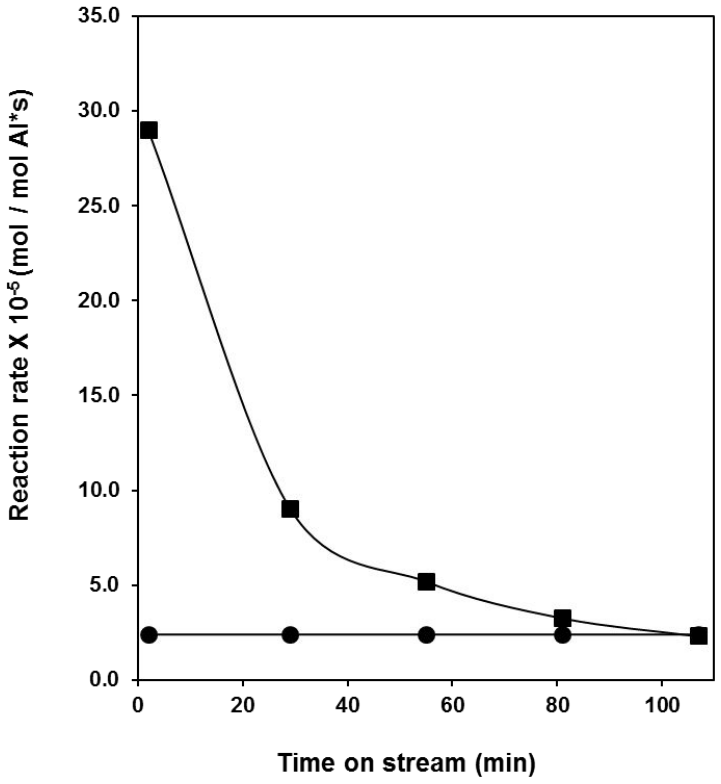

Figure S.1: C_3H_8 dehydrogenation rates (filled squares) and cracking rates (filled circles) as a function of time-on-stream, measured at 1.4 kPa C_3H_8/He and τ = 10 mol Al*s/mol C_3H_8 space time and 733 K. C_3H_8 conversions were < 2 %

Text S2.

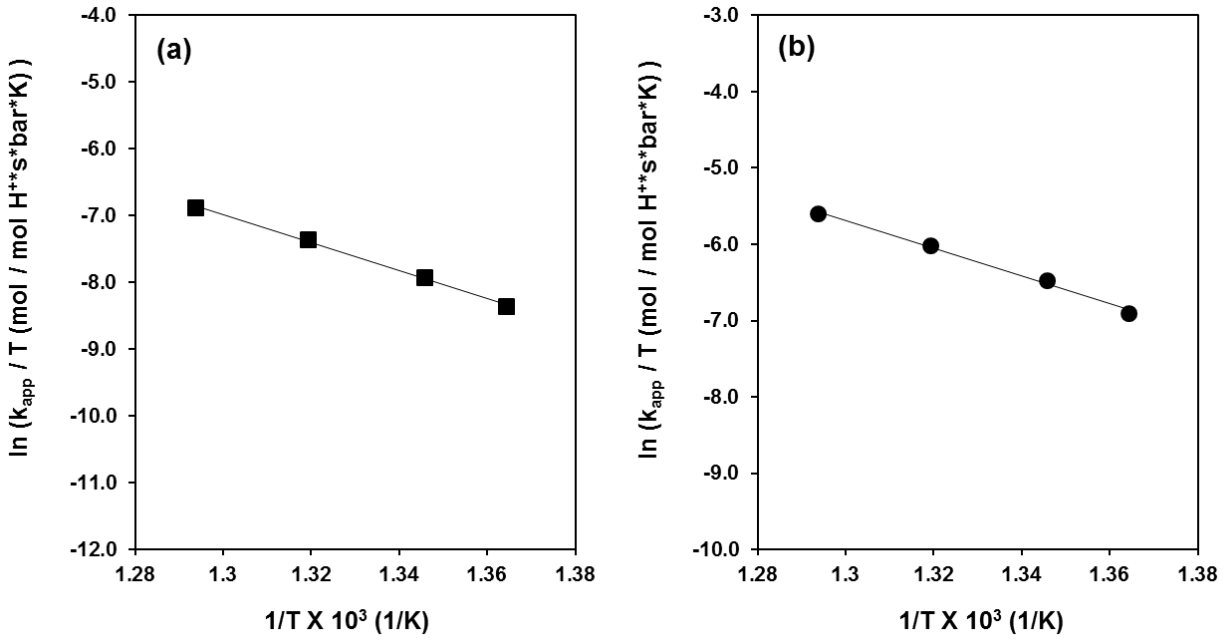

Figure S.2: First-order rate coefficients (k_{app}) for C_3H_8 dehydrogenation (a) and cracking (b) as a function of temperature. Rate constants were normalized to the density of Brønsted acid O-H acid groups in H-MFI, measured via NH_3 –TPD (0.87 H^+/Al_{tot}).

Text S3. Effects of space time on steady-state product selectivities over Ga/H-MFI (Ga/Al = 0.2) during C_3H_8 conversion

Shown in Figure S3, are the steady-state product selectivities (shown as % of converted C in products) as a function of space time for the reaction of C_3H_8 over Ga/H-MFI (Ga/Al =0.2) at 733 K and 1.5kPa C_3H_8/He. Under the differential conversions employed during reactivity measurements (< 7% C_3H_8 conversion), only C_3H_6, CH_4, C_2H_4 and aromatics (C_6H_6 and C_7H_8) were detected as reaction products in the reactor effluent. All product selectivities shown in Figure S3 were also linearly extrapolated to 0 space time, as can be seen by the dotted lines in the figure. C_3H_6 is the dominant product at all space times tested (> 85% C selectivity), but the selectivity to this product decreases with increasing space time from an extrapolated C selectivity of 96 % at 0 space time. The decrease in C_3H_6 selectivity with increasing space time is attributed to secondary pathways that consume C_3H_6 to form higher molecular weight products, such as aromatics. The C selectivity to C_2H_4 is about 3% at zero space time and then increases linearly with increasing space time. By contrast the C selectivity to CH_4 is roughly independent of space time, with a value of approximately 1.5%. The ratio of the extrapolated C selectivities of C_2H_4 and CH_4 (approximately 2) is consistent with the cracking of C_3H_8 into C_2H_4 and CH_4. The increase in this ratio with increasing space time that additional C_2H_4 is formed by the cracking of higher molecular weight products. This could occur, for example, via β-scission of larger alkenes. The C selectivity to aromatics (C_6H_6 and C_7H_8) increased with increasing space time and at zero space time, extrapolated to a value close to zero, suggesting that these products form via secondary pathways from products of C_3H_8 dehydrogenation and cracking. This trend is consistent with previous experiments studies of C_3H_8 conversion over Ga/H-MFI.[1]

Measured selectivities of products (on a C_3H_8 basis) together with overall C_3H_8 conversion rates were used to determine the rates of C_3H_8 dehydrogenation, cracking and aromatics formation. These rates are shown as a function of space time in Figure S4a-d. The rate of C_3H_8 consumption (Figure S4a) decreases with increasing space time, possibly due to inhibition by the products of C_3H_8 conversion. To explore this possibility, reaction rates were also measured in the presence of co-fed H_2. In the presence of 1.5kPa H_2, the rates of C_3H_8 conversion (open symbols in Figure S4a) show a much weaker dependence on space time, confirming that H_2 inhibits the rates. C_3H_8 dehydrogenation rates (Figure S4b) and C_3H_8 cracking rates (Figure S4c) also decrease with increasing space time. In the presence of 1.5kPa cofed H_2, both rates show a much weaker dependence on space time. We note that while the inhibition of the rate of C_3H_8 dehydrogenation by H_2 has been reported in previously,[1,2] inhibition of the rate of C_3H_8 cracking rate by H_2 has not been reported. We note that H_2 does not inhibit Brønsted acid catalyzed monomolecular dehydrogenation and cracking on H-MFI. This observation suggests that the site requirements for both the dehydrogenation and cracking reaction over Ga/H-MFI are similar i.e., both reactions may be catalyzed by Ga^{3+} sites. Both rates also exhibit a weak, but observable decrease with space time, even in the presence of 1.5kPa H_2. We speculate that this residual inhibition arises from the binding of alkene products to Ga^{3+} sites. Aromatics formation rates (Figure S4d) increased with space time, consistent with their secondary nature. The formation of aromatics was, however, strongly inhibited by H_2, suggesting that their formation also requires the participation of Ga^{3+} sites.

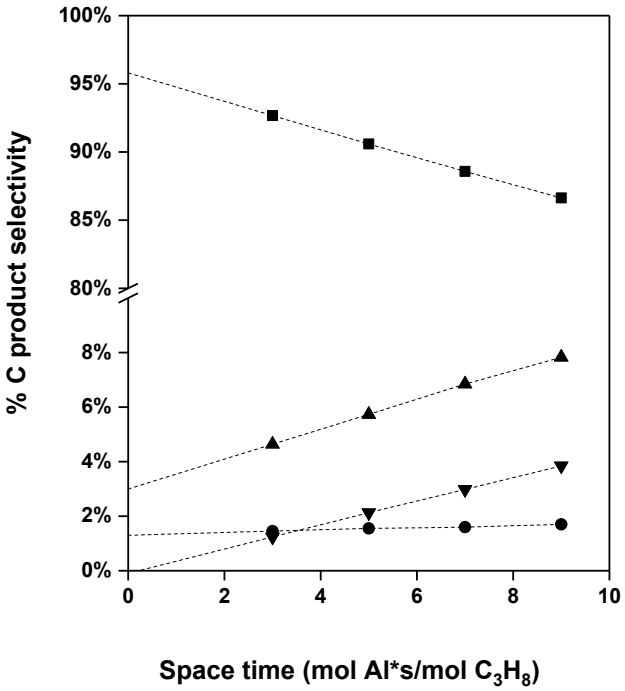

Figure S3: C product selectivities (% of C converted to products) as a function of space time, during C_3H_8 conversion over Ga/H-MFI (Ga/Al =0.2) at 1.5 kPa C_3H_8/He and 733 K. Ga/H-MFI was pre-treated in 2.5% H_2/He at 773 K, prior to reaction. C_3H_8 conversions were < 9 %. Filled squares (■) denote C_3H_6, filled triangles (▲) denote C_2H_4, filled inverted triangles (▼) denote aromatics (C_6H_6 and C_7H_8) and filled circles (●) denote CH_4. Dotted lines indicate linear extrapolations to 0 space time.

Table S1: Apparent reaction orders of H_2 for C_3H_8 dehydrogenation and cracking at 0.9 kPa C_3H_8 and 8 kPa C_3H_8 measured at 733 K over Ga/Al = 0.2. Data are derived from Figure 6.

C_3H_8 partial pressure X 10^2 (bar)	Dehydrogenation	Cracking
0.9	-0.3	-0.5
8.0	-0.1	-0.1

[a] Apparent reaction orders were determined using the relationship Rate = $k[H_2]^X$ where k is a rate coefficient and x is the reaction order

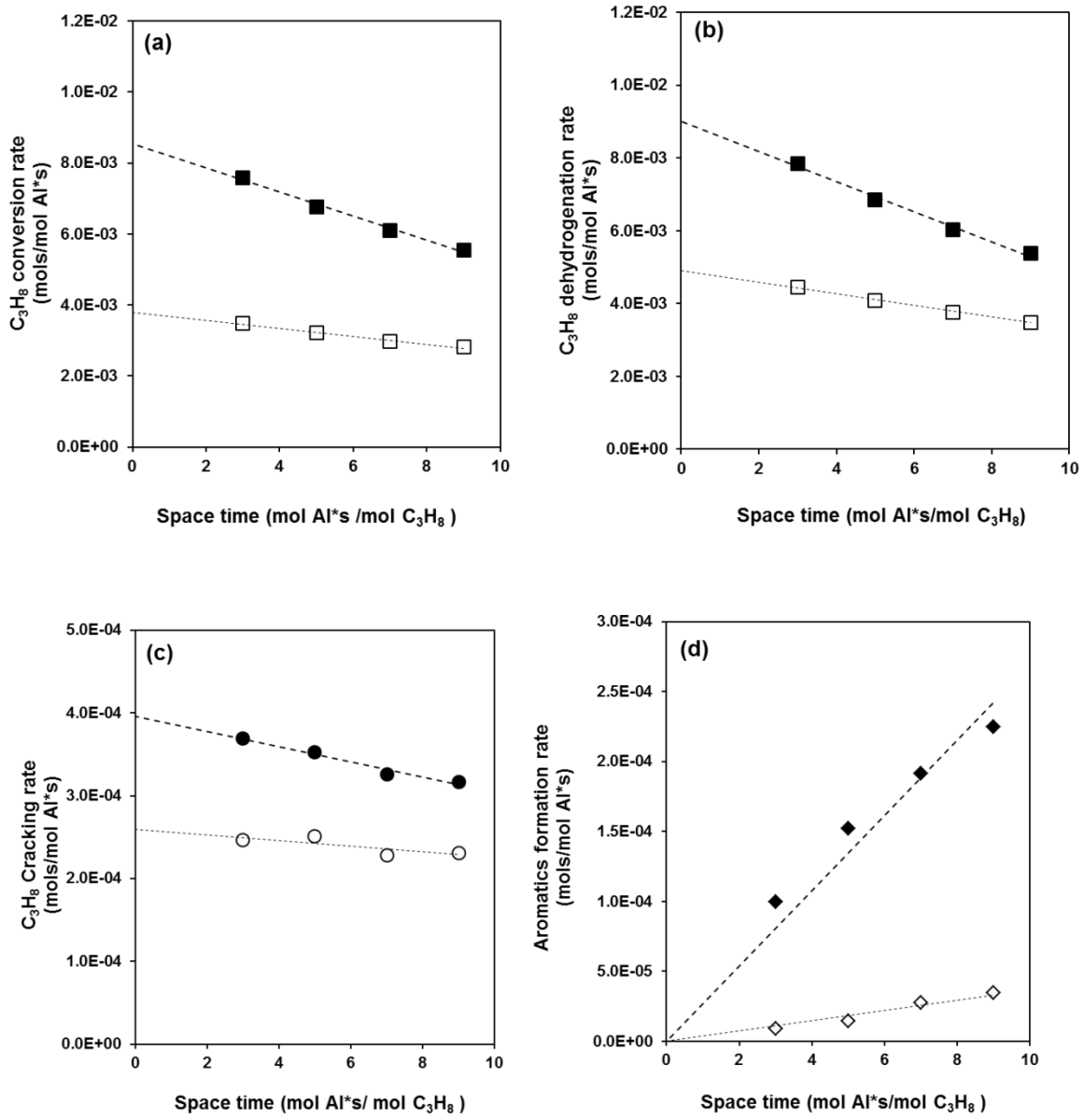

Figure S4: (a) C_3H_8 conversion rates (per Al_{tot} atom) as a function of space time. (b) C_3H_8 dehydrogenation rates (per Al_{tot} atom) as a function of space time. (c) C_3H_8 cracking rates (per Al_{tot} atom) as a function of space time. (d) Aromatics (C_6H_6 and C_7H_8) formation rates (per Al_{tot} atom) as a function of space time. In all plots, closed symbols refer to 0 kPa cofed H_2 and open symbols refer to 1.5 kPa cofed H_2. Rates were measured at 1.5 kPa C_3H_8/He at 733 K.

Text S.4 Derivation of rate equations for plausible mechanisms for dehydrogenation and cracking over Ga/H-MFI.

(a) Derivation of rate law for C_3H_8 dehydrogenation over $[GaH]^{2+}$ sites via alkyl mechanism

The elementary steps outlined in Scheme 1 for C_3H_8 dehydrogenation over $[GaH]^{2+}$ sites are used here to derive a rate law in terms of kinetic and thermodynamic coefficients. The steady-state hypothesis was applied to all reactive surface intermediates. On the basis of free energy and enthalpy calculations outlined in Figure S.5, the physisorption of C_3H_8 onto $[GaH]^{2+}$ to form C_3H_8-$[GaH]^{2+}$ complexes (Step 1) and the dissociative adsorption of C_3H_8-$[GaH]^{2+}$ to form $[C_3H_7\text{-}GaH]^{+}$-H^{+} cation pairs (Step 2) are predicted to have low activation barriers ($\leq$ 2 kcal/mol) and are therefore assumed to be quasi-equilibrated. This assumption leads to the derivation of equations S1 and S2 that describe the relationship between gas-phase C_3H_8 and C_3H_8 derived surface intermediates.

$$K_{phys} = \frac{[C_3H_8 - [GaH]^{2+}]}{[C_3H_8][GaH]^{2+}} \quad \text{S1}$$

$$K_{dis} = \frac{[[C_3H_7 - GaH]^{+} - H^{+}]}{[C_3H_8 - [GaH]^{2+}]} \quad \text{S2}$$

Here, K_{phys} and K_{dis} are the thermodynamic adsorption constants for C_3H_8 physisorption at $[GaH]^{2+}$ and dissociation of C_3H_8 by $[GaH]^{2+}$ into $[C_3H_7Ga\text{-}H]^{+}$-H^{+} cation pairs, respectively. Similarly, inhibition of reaction rates by H_2 may occur via dissociation of H_2 by $[GaH]^{2+}$ to form $[GaH_2]^{+}$-H^{+} pairs as described by equation S3.

$$K_{H_2} = \frac{[[GaH_2]^+ - H^+]}{[H_2][GaH]^{2+}} \quad \text{S3}$$

Here, K_{H2} is the equilibrium constant for H_2 dissociation.

As also described in the main text, the rate-limiting step in the alkyl dehydrogenation sequence is the cyclic β-hydride elimination of C_3H_7 fragments by the Ga^{3+} center to form C_3H_6 and H_2 in a concerted step (Step 3). The overall rate of dehydrogenation (per $[GaH]^{2+}$) can be described by equation S4.

$$\frac{\text{Rate, D}}{[GaH]^{2+}} = k_{alk}\theta_{alk} \quad \text{S4}$$

Here, Rate, D refers to the dehydrogenation rate, k_{alk} refers to the rate coefficient for β-hydride elimination and θ_{alk} refers to the surface coverage of $[C_3H_7\text{-}GaH]^+\text{-}H^+$ cation pairs, the precursor to the rate-limiting transition state and is given by equation S5.

$$\theta_{alk} = \frac{[[C_3H_7 - GaH]^+ - H^+]}{[L]} \quad \text{S5}$$

Here, $[[C_3H_7\text{-}GaH]^+\text{-}H^+]$ refers to the surface concentration of $[C_3H_7\text{-}GaH]^+\text{-}H^+$ cation pairs and [L] refers to the total density of active sites i.e $[GaH]^{2+}$ sites. [L] can be described in terms of the various reactive surface intermediates via equation S6.

$$[L] = [GaH]^{2+} + [C_3H_8\text{-}[GaH]^{2+}] + [[C_3H_7\text{-}GaH]^+\text{-}H^+] + [[GaH_2]^+\text{-}H^+] \quad \text{S6}$$

Theoretical calculations suggest that the interaction of gas-phase C_3H_8 with $[GaH]^{2+}$ is expected to be weak (~ - 6kcal/mol adosorption enthalpy) . Therefore the second term in equation S6 can be neglected. This leads to a reduction in equation S6 to equation S7.

$$[L] = [GaH]^{2+} + [[C_3H_7\text{-}GaH]^{+}\text{-}H^{+}] + [[GaH_2]^{+}\text{-}H^{+}] \quad \text{S7}$$

Solving equations S1-S7 leads to a rate expression for C_3H_8 dehydrogenation, shown below as equation S8, shown in the main text as equation 3.

$$\frac{\text{Rate, D}}{[GaH]^{2+}} = \frac{k_{alk}K_{dis}K_{phys}[C_3H_8]}{1 + K_{dis}K_{phys}[C_3H_8] + K_{H_2}[H_2]} \quad \text{S8}$$

(b) Derivation of rate law for C_3H_8 dehydrogenation over $[GaH]^{2+}$ sites via carbenium mechanism.

The elementary steps outlined in Scheme 2 for C_3H_8 dehydrogenation over $[GaH]^{2+}$ sites are used here to derive a rate law in terms of kinetic and thermodynamic coefficients. The steady-state hypothesis was applied to all reactive surface intermediates. As discussed in Text S.4 (a), we assumed the physisorption of C_3H_8 over $[GaH]^{2+}$ sites to form $[C_3H_8\text{-}[GaH]^{2+}]$ complexes (Step 1) is quasi-equilibrated. Theoretical calculations suggest that that rate-limiting step for the carbenium mechanism is the activation of the α C-H bond in C_3H_8 , resulting in a hydride transfer to the Ga^{3+} center and concomitant formation of a propyl carbenium fragment (Step 2). Accordingly, the dehydrogenation rate (per $[GaH]^{2+}$) can be expressed as equation S9.

$$\frac{\text{Rate, D}}{[GaH]^{2+}} = k_{carb}\theta_{phys} \quad \text{S9}$$

Here, Rate, D refers to the dehydrogenation rate, k_{carb} refers to the rate coefficient for α C-H carbenium activation and θ_{phys} refers to the surface coverage of $[C_3H_8\text{-}[GaH]^{2+}]$ complexes, the precursor to the rate-limiting transition state and is given by equation S10.

$$\theta_{phys} = \frac{[C_3H_8 - [GaH]^{2+}]}{[L]} \qquad S10$$

Here, $[C_3H_8\text{-}[GaH]^{2+}]$ refers to the surface concentration of $C_3H_8\text{-}[GaH]^{2+}$ complexes and [L] refers to the total density of active sites i.e $[GaH]^{2+}$ sites. [L] can be described in terms of the various reactive surface intermediates via equation S11. Inhibition by H_2 can be described via the formation of $[GaH_2]^+\text{-}H^+$ cation pairs, as shown in equation S3.

$$[L] = [GaH]^{2+} + [C_3H_8\text{-}[GaH]^{2+}] + [[GaH_2]^+\text{-}H^+] \qquad S11$$

Since the interaction of gas-phase C_3H_8 with $[GaH]^{2+}$ cations is predicted to be weak, the second term in equation S11 can be neglected. Together with equations S1, S9-S11, a rate law for dehydrogenation via the carbenium mechanism can be derived, shown as equation S12 here and as equation 4 in the main text.

$$\frac{\text{Rate, D}}{[GaH]^{2+}} = \frac{k_{carb}K_{phys}[C_3H_8]}{1 + K_{H_2}[H_2]} \qquad S12$$

It can be seen from equation S12, that in the absence of cofed H_2 at very low H_2 concentrations, equation S12 reduces to equation S13, which predicts the dehydrogenation rate to bear a first-order dependence on C_3H_8 at all C_3H_8 partial pressures.

$$\frac{\text{Rate, D}}{[GaH]^{2+}} = \frac{k_{carb}K_{phys}[C_3H_8]}{1} \qquad S13$$

(b) Derivation of rate law for C_3H_8 cracking over $[GaH]^{2+}$ sites via alkyl mechanism.

The elementary steps outlined in Scheme 3 for C_3H_8 cracking over $[GaH]^{2+}$ sites can be used to derive a rate expression containing kinetic and thermodynamic coefficients that describes the dependence of cracking rates on C_3H_8 and H_2 partial pressures. Equations S1, S2 and S3 also describe the surface intermediates relevant for C_3H_8 cracking, as outlined in Scheme 3. Theoretical calculations predict that the rate-limiting step for C_3H_8 cracking is the C-C bond attack of the anionic C_3H_7 fragment by the proximate Brønsted acid O-H group that constitutes the $[C_3H_7\text{-}GaH]^+\text{-}H^+$ cation pair (Step 3). Therefore, the rate of C_3H_8 cracking (per $[GaH]^{2+}$) can be expressed as equation S14.

$$\frac{\text{Rate, C}}{[\text{GaH}]^{2+}} = k_{crack}\theta_{alk} \qquad \text{S14}$$

Here, Rate, C refers to the C_3H_8 cracking rate, k_{crack} refers to the rate coefficient for C-C bond attack in Step 4 and θ_{alk} refers to the surface coverage of $[C_3H_7\text{-}GaH]^+\text{-}H^+$ cation pairs, the precursor to the cracking transition state. θ_{alk} can be described by equations S5-S7. Together, these equations lead to a rate expression for C_3H_8 cracking over $[GaH]^{2+}$ sites, in terms of C_3H_8 and H_2 partial pressures, shown as equation S15 here and equation 5 in the main text.

$$\frac{\text{Rate, C}}{[\text{GaH}]^{2+}} = \frac{k_{crack}K_{dis}K_{phys}[C_3H_8]}{1 + K_{dis}K_{phys}[C_3H_8] + K_{H_2}[H_2]} \qquad \text{S15}$$

Text S.5 Derivations of equations relating experimentally measured rate coefficients to apparent and intrinsic activation enthalpies

Both dehydrogenation and cracking rates over Ga/H-MFI obey the behavior predicted by a Langmuir Hinshelwood kinetic model, shown in Equations 1 and 2 of the main text. At very low C_3H_8 pressures, experimentally observed dehydrogenation and cracking rates bear a first-order dependence on C_3H_8 pressure. The rate coefficient for this first order dependence (k_{app}) bears units of (mol/ mol Al*s*bar) can therefore be expressed as a product of an intrinsic, zero-order rate coefficient (k_{int}) with units of (mol/ mol Al*s) and a thermodynamic adsorption constant (K_{ads}) with units of (bar^{-1}), as shown in Equation S16[3]

$$k_{app} = k_{int} * K_{ads} \qquad \text{S17}$$

Here, the intrinsic rate coefficient k_{int} which purely reflects the dynamics between the transition state and the adsorbed state directly preceding it can be expressed with the aid of classical transition-state theory as Equation S18.[4]

$$k_{int} = \frac{\kappa k_B T}{h} \exp\left(-\frac{\Delta G_{int}}{RT}\right) \qquad \text{S18}$$

Here, k_{int} is the instrinsic rate constant (s^{-1}), κ is the transmission coefficient, k_B is the Boltzmann constant, h is the Planck constant, T is temperature (K), ΔG_{int} is the intrinsic Gibbs free energy activation barrier, R is the gas constant.

The thermodynamic adsorption constant K_{ads} which relates gas-phase C_3H_8 to the adsorbed state preceding the transition state can be expressed in terms of the Gibbs free energy of adsorption as Equation S19.[3]

$$K_{ads} = \exp\left(-\frac{\Delta G_{ads}}{RT}\right) \qquad \text{S19}$$

The Gibbs free energy can be expressed in terms of enthalpy (ΔH) and entropy (ΔS), as shown in Equation S20

$$\Delta G = \Delta H - T\Delta S \qquad \text{S20}$$

Combining Equations S17-S19 leads to Equation S21

$$k_{app} = \frac{k_B T}{h}\exp\left(-\frac{\Delta G_{int}}{RT}\right)\exp\left(-\frac{\Delta G_{ads}}{RT}\right) \qquad \text{S21}$$

Further simplification of Equation S21 leads to Equation S22

$$k_{app} = \frac{k_B T}{h}\exp\left(-\frac{(\Delta G_{int} + \Delta G_{ads})}{RT}\right) \qquad \text{S22}$$

Equations S22 suggests that the apparent first order rate coefficient reflects the the Gibbs free energy of activation with respect to gas-phase C_3H_8 (ΔG_{app}), as also summarized in Scheme 4 of the main text. This finding can be summarized as Equation S23.

$$\Delta G_{app} = \Delta G_{int} + \Delta G_{ads} \qquad \text{S23}$$

Combining Equation S20 with Equation S22 and S23, the first order rate coefficient can be expressed in terms of the apparent activation enthalpy (ΔH_{app}) and entropy (ΔS_{app}) , shown here as Equation S24

$$\ln\left(\frac{k_{app}}{T}\right) = -\frac{\Delta H_{app}}{RT} + \frac{\Delta S_{app}}{R} + \ln\left(\frac{k_B}{h}\right) \qquad \text{S24}$$

Similarly, Equation S18 together with Equation S20 can be used to express the intrinsic rate coefficient (k_{int}) in terms of the intrinsic activation enthalpy (ΔH_{int}) and entropy (ΔS_{int}) , shown here as Equation S25

$$\ln\left(\frac{k_{int}}{T}\right) = -\frac{\Delta H_{int}}{RT} + \frac{\Delta S_{int}}{R} + \ln\left(\frac{k_B}{h}\right) \qquad \text{S25}$$

Finally, the thermodynamic adsorption constant (K_{ads}) can be expressed in terms of the adsorption enthalpy (ΔH_{ads}) by combining Equation S19 and S20, shown here as Equation S26

$$\ln\left(K_{ads}\right) = -\frac{\Delta H_{ads}}{RT} + \frac{\Delta S_{ads}}{R} \qquad \text{S26}$$

Plots of $\ln(k_{int}/T)$ vs $1/T$ lead to the extraction of ΔH_{app} , ΔH_{int} and ΔH_{ads} via linear regression methods. These plots are presented for dehydrogenation and cracking in Figures S10, S11 and S12.

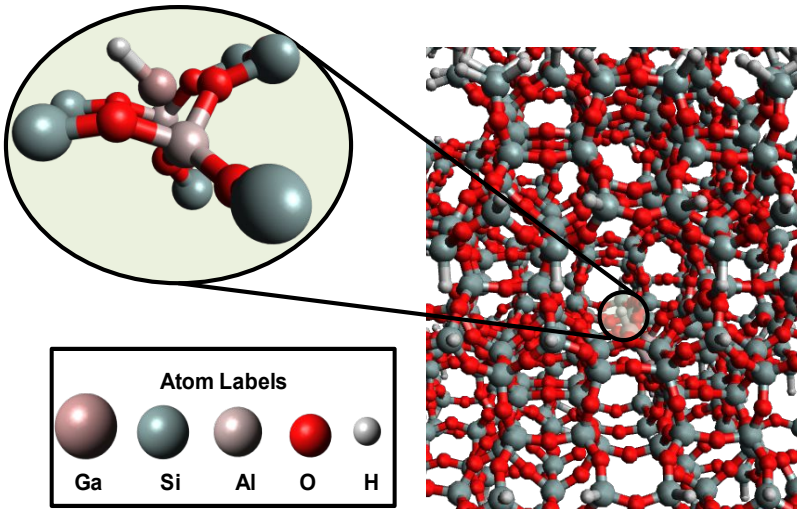

Figure S5. View along [100] axis of T437 atom MFI structure used to model $[GaH]^{2+}$ sites in Ga/H-MFI. The QM region consists of a T9 model which is electrostatically embedded in an MM region

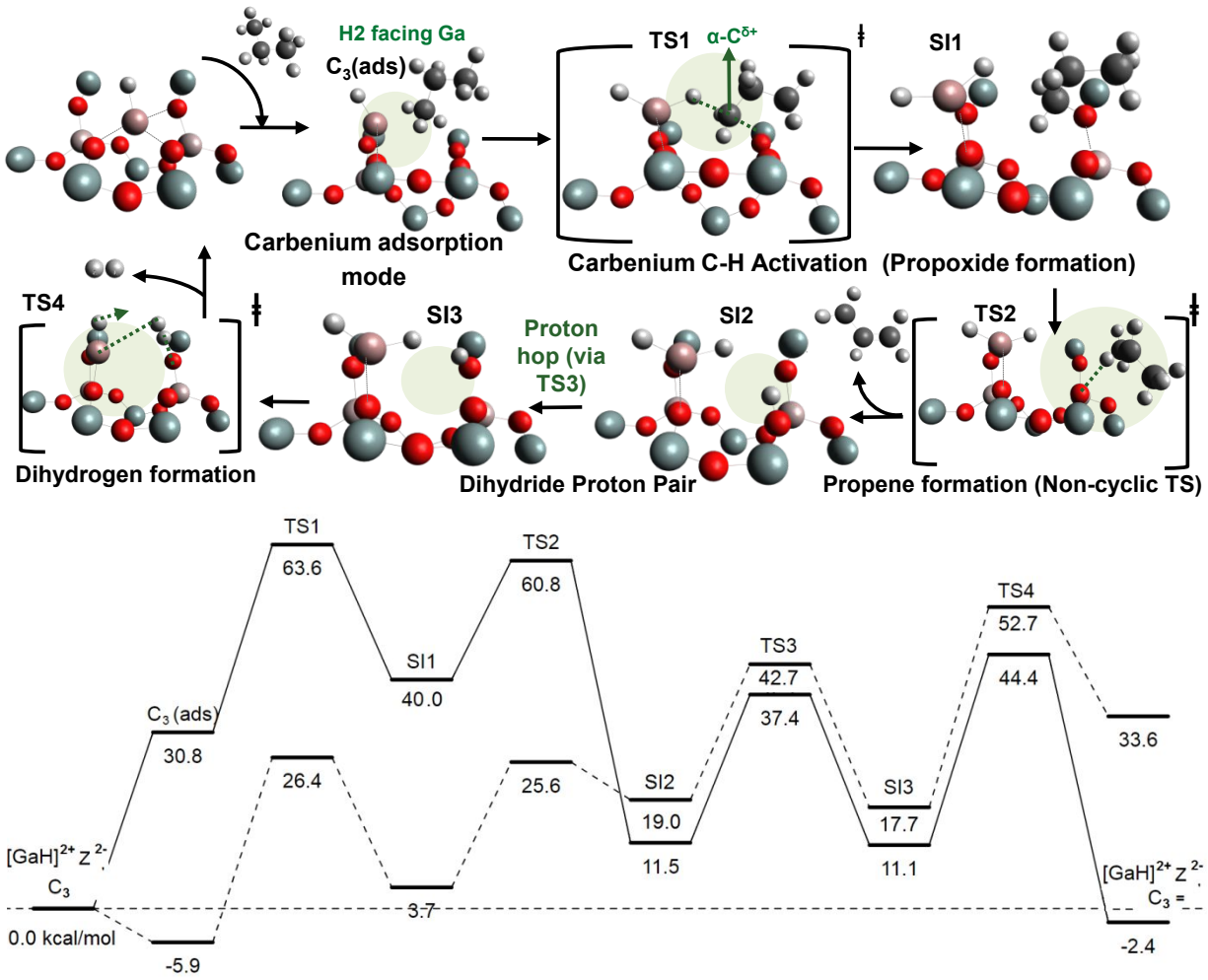

Figure S6. Free Energy (full lines) and enthalpy (dashed lines) landscapes for C_3H_8 dehydrogenation via carbenium mechanism on $[GaH]^{2+}$ sites, reported at 733 K, 10 kPa C_3H_8, 0.5 kPa C_3H_6 and 0.5 kPa H_2. Only the QM region from the QM/MM model has been displayed here to illustrate the elementary steps in this mechanism, using the key from Figure S5.

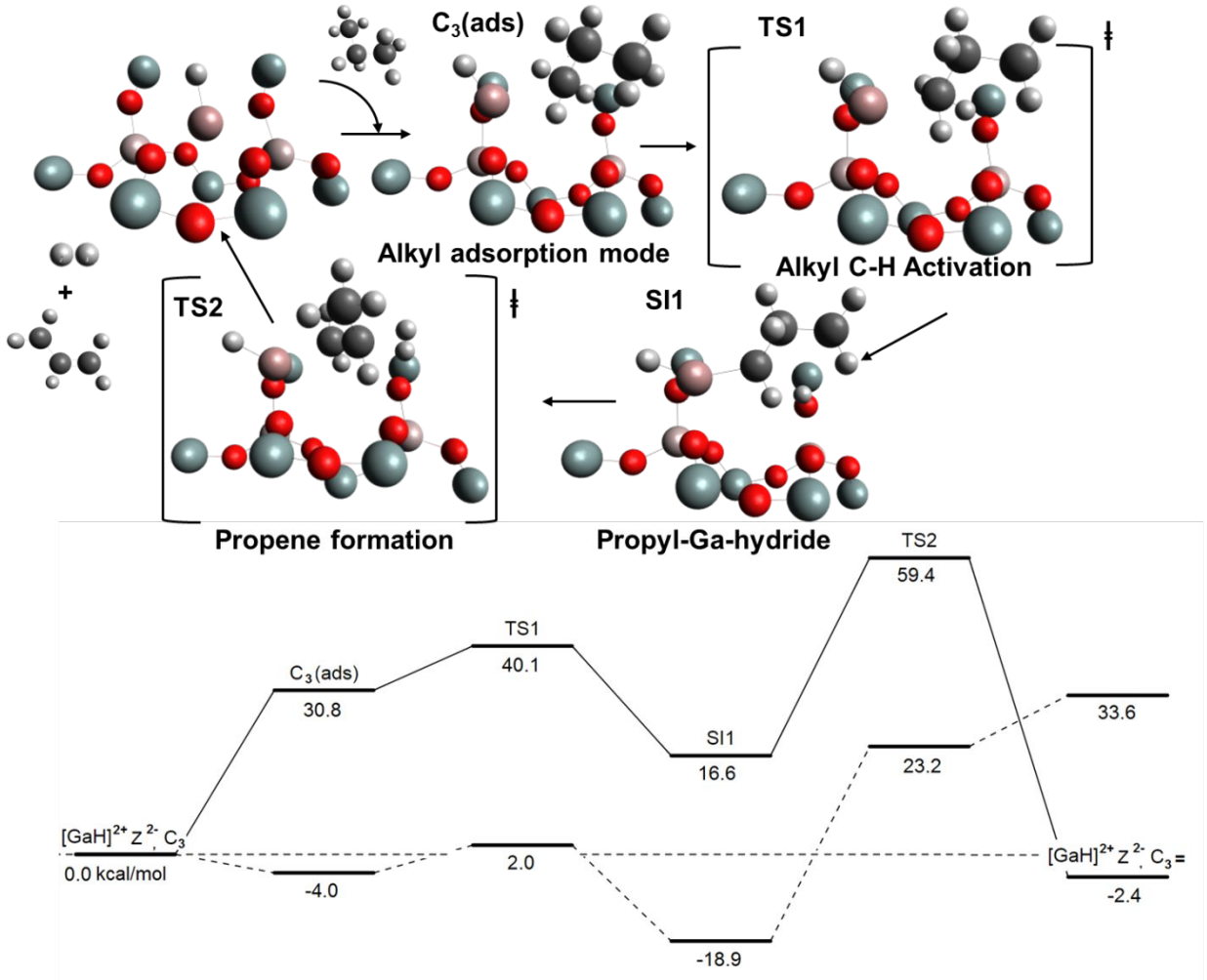

Figure S7. Free Energy (full lines) and enthalpy (dashed lines) landscapes for C_3H_8 dehydrogenation via alkyl mechanism on $[GaH]^{2+}$ sites, reported at 733 K, 10 kPa C_3H_8, 0.5 kPa C_3H_6 and 0.5 kPa H_2. Only the QM region from the QM/MM model has been displayed here to illustrate the elementary steps in this mechanism, using the key from Figure S5.

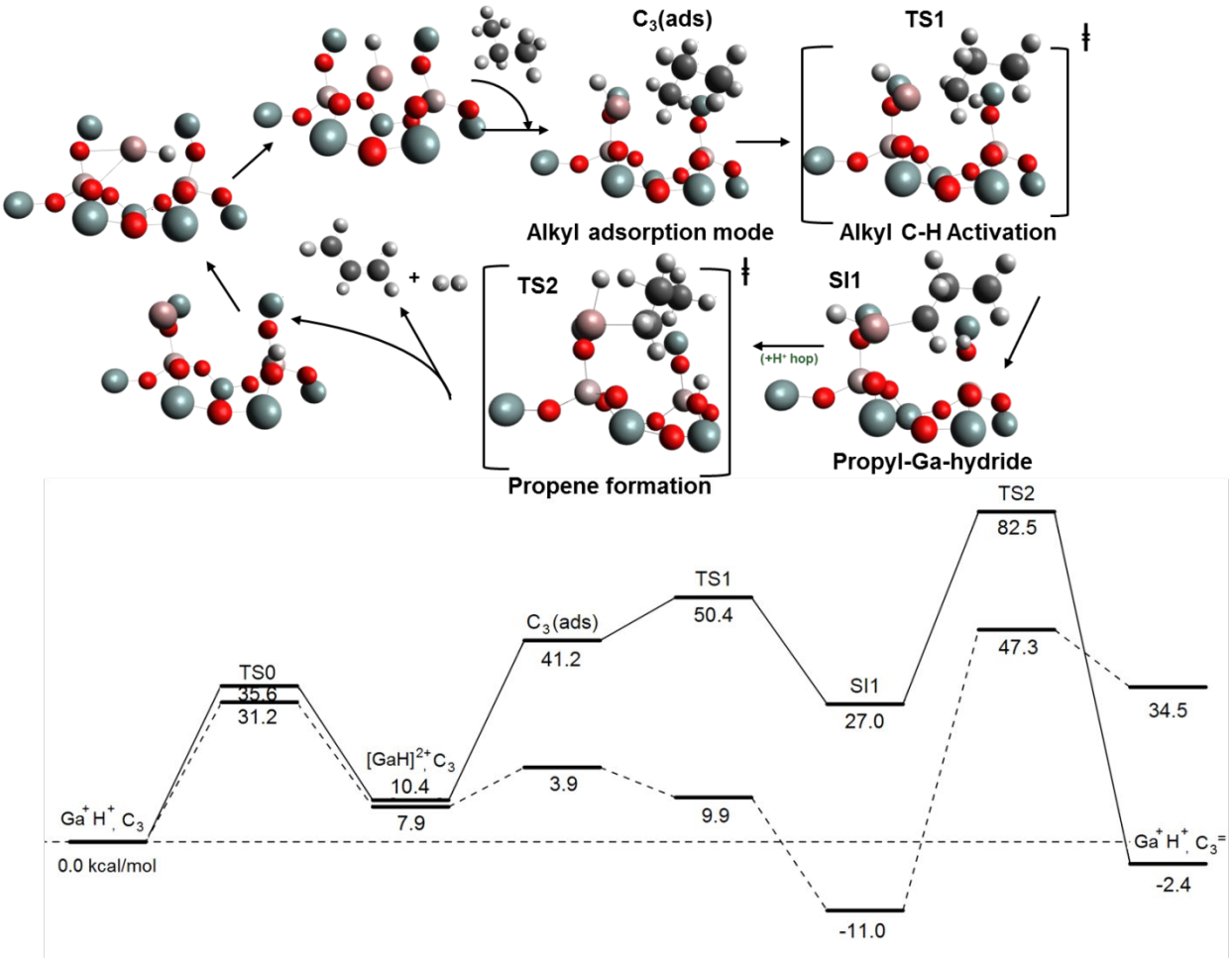

Figure S8. Free Energy (full lines) and enthalpy (dashed lines) landscapes for C_3H_8 dehydrogenation on Ga^+- H^+ sites, reported at 733 K, 10 kPa C_3H_8, 0.5 kPa C_3H_6 and 0.5 kPa H_2. Only the QM region from the QM/MM model has been displayed here to illustrate the elementary steps in this mechanism, using the key from Figure S5.

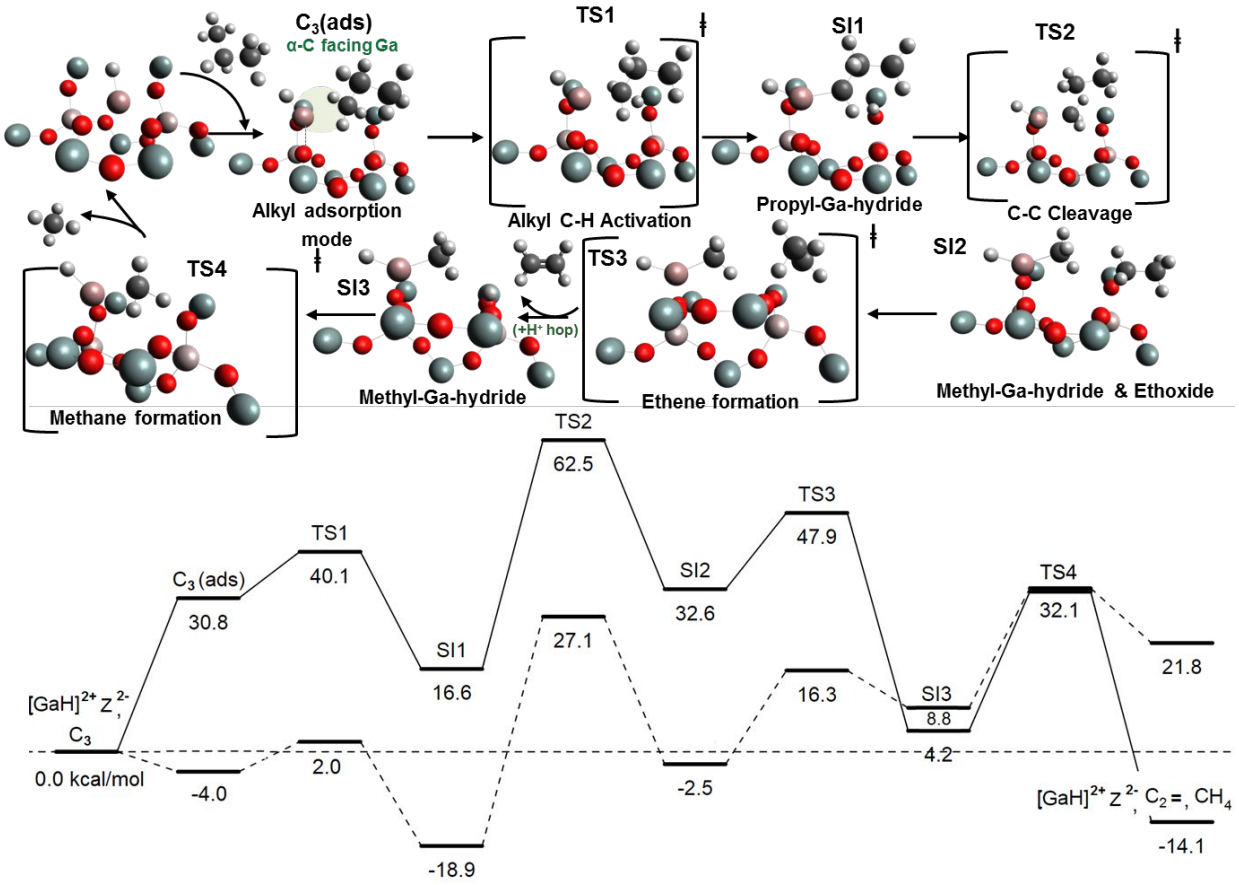

Figure S9. Free Energy (full lines) and enthalpy (dashed lines) landscapes for C_3H_8 cracking via alkyl mechanism on $[GaH]^{2+}$ sites, reported at 733 K, 10 kPa C_3H_8, 0.5 kPa C_2H_4, and 0.5 kPa CH_4. Only the QM region from the QM/MM model has been displayed here to illustrate the elementary steps in this mechanism, using the key from Figure S5.

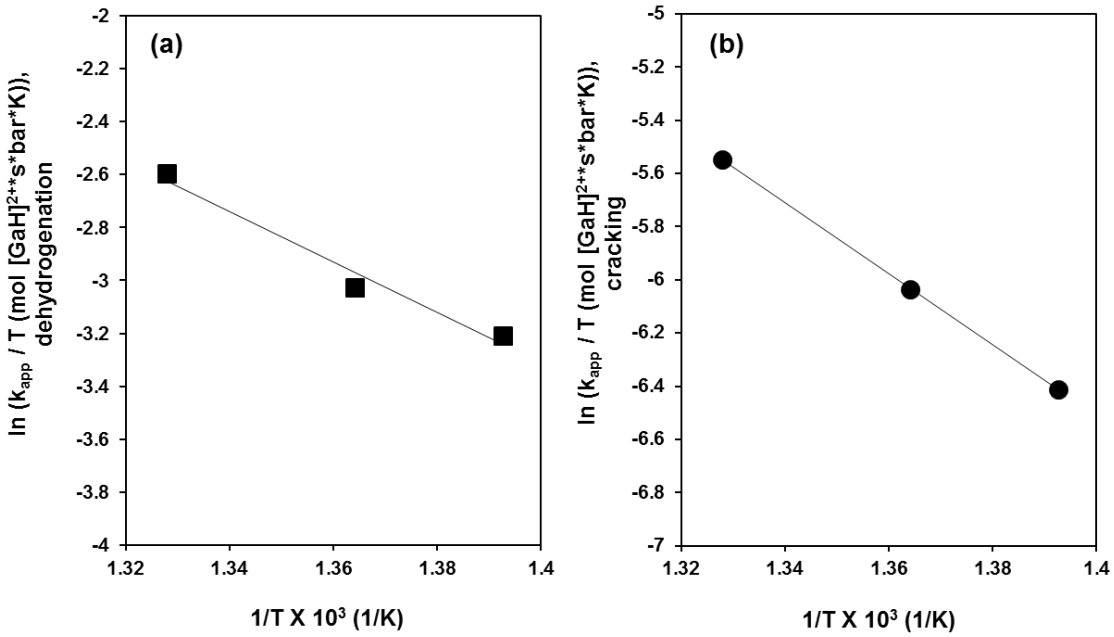

Figure S10: Plots of ln (k_{app} /T) vs 1/T for (a) C_3H_8 dehydrogenation (b) C_3H_8 cracking for the Ga/Al = 0.2 sample. Values for k_{app} (first order rate coefficients) were obtained by regression of rate data in Figures 5a-c and 6a-c to Equations 1 and 2. Rate coefficients were normalized to the fraction of $[GaH]^{2+}$ sites per Al_{tot} estimated via NH_3-TPD.[5]Solid lines reflect linear regression to Equation S24

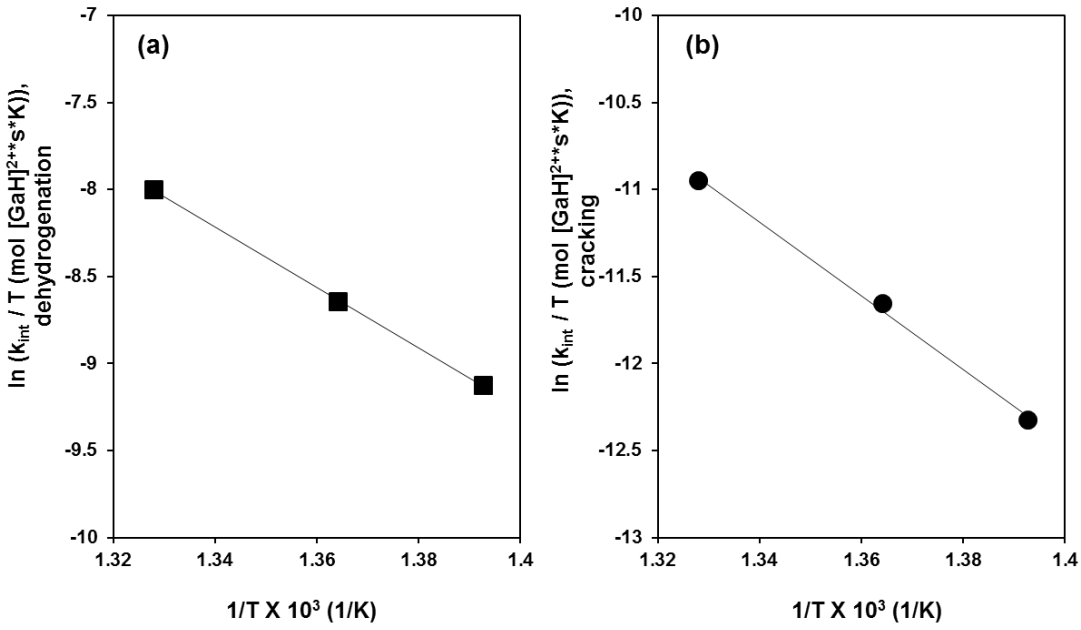

Figure S11: Plots of ln (k_{int} /T) vs 1/T for (a) C_3H_8 dehydrogenation (b) C_3H_8 cracking for the Ga/Al = 0.2 sample. Values for k_{int} (zero order rate coefficients) were obtained by regression of rate data in Figures 5a-c and 6a-c to Equations 1 and 2. Rate coefficients were normalized to the fraction of $[GaH]^{2+}$ sites per Al_{tot} estimated via NH_3-TPD.[5]Solid lines reflect linear regression to Equation S25.

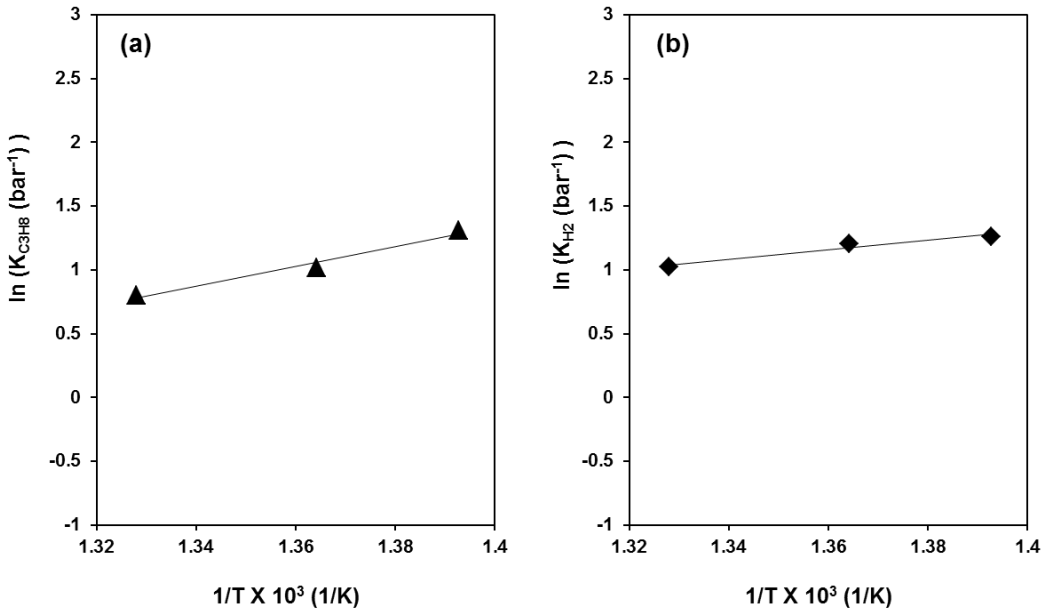

Figure S12: Plots of ln (K_{ads}) vs 1/T for (a) C_3H_8 adsorption (b) H_2 adsorption for the Ga/Al = 0.2 sample. Values for K_{ads} (adsorption constants) were obtained by regression of rate data in Figures 5a-c and 6a-c to Equations 1 and 2.Solid lines reflect linear regression to Equation S26.

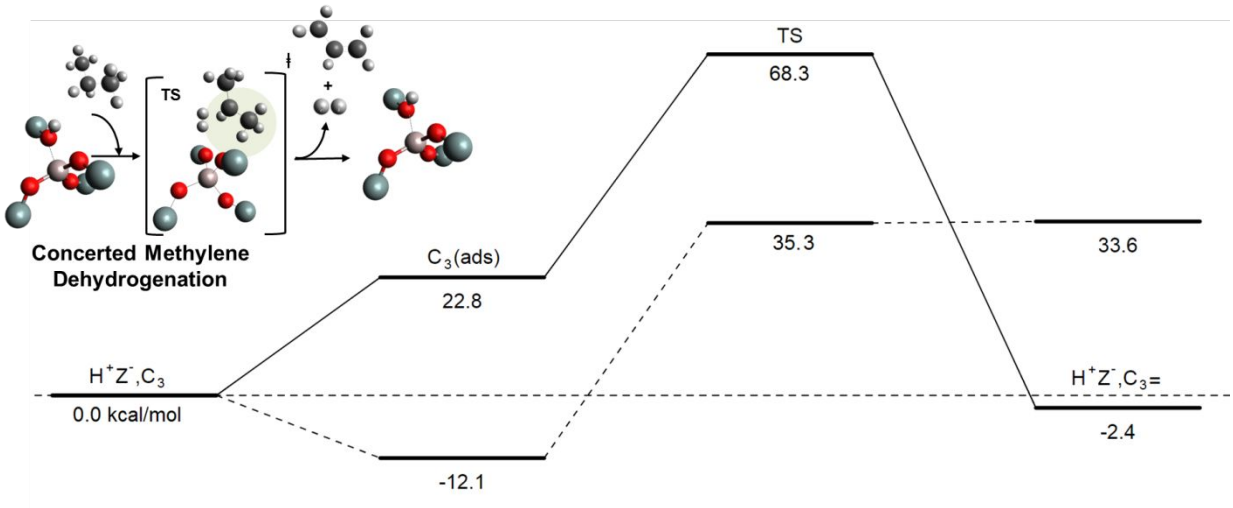

Figure S13. Free Energy (full lines) and enthalpy (dashed lines) landscapes for C_3H_8 dehydrogenation (methylene) on Brønsted acid O-H groups, reported at 733 K, 10 kPa C_3H_8, 0.5 kPa C_3H_6 and 0.5 kPa H_2. Only the QM region from the QM/MM model has been displayed here to illustrate the elementary steps in this mechanism, using the key from Figure S5.

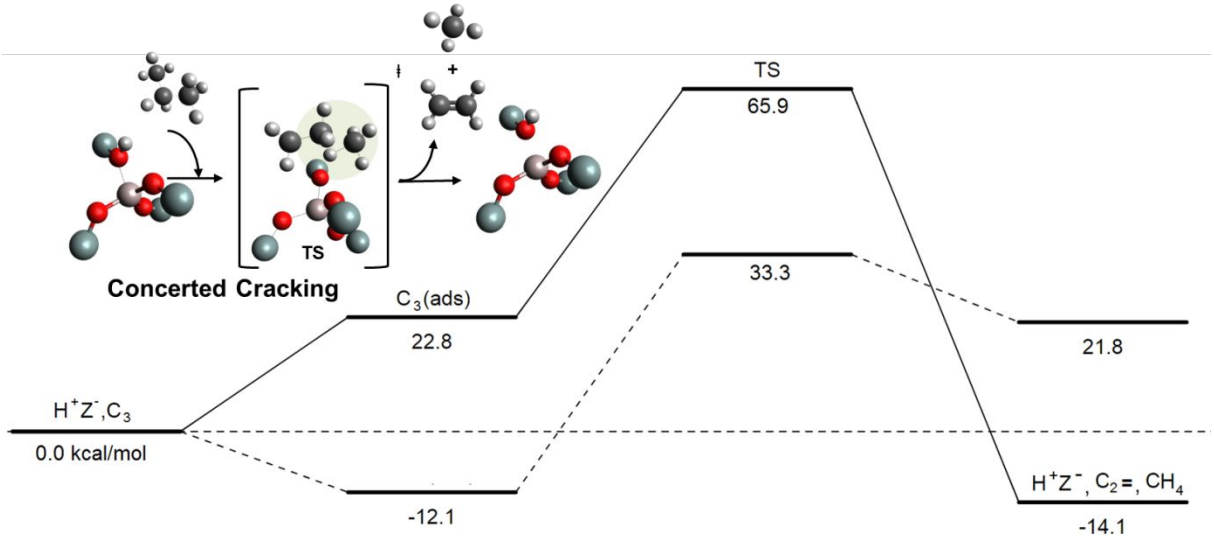

Figure S14. Free Energy (full lines) and enthalpy (dashed lines) landscapes for C_3H_8 cracking catalyzed by Brønsted acid O-H groups, reported at 733 K, 10 kPa C_3H_8, 0.5 kPa C_2H_4, and 0.5 kPa CH_4. Only the QM region from the QM/MM model has been displayed here to illustrate the elementary steps in this mechanism, using the key from Figure S5.

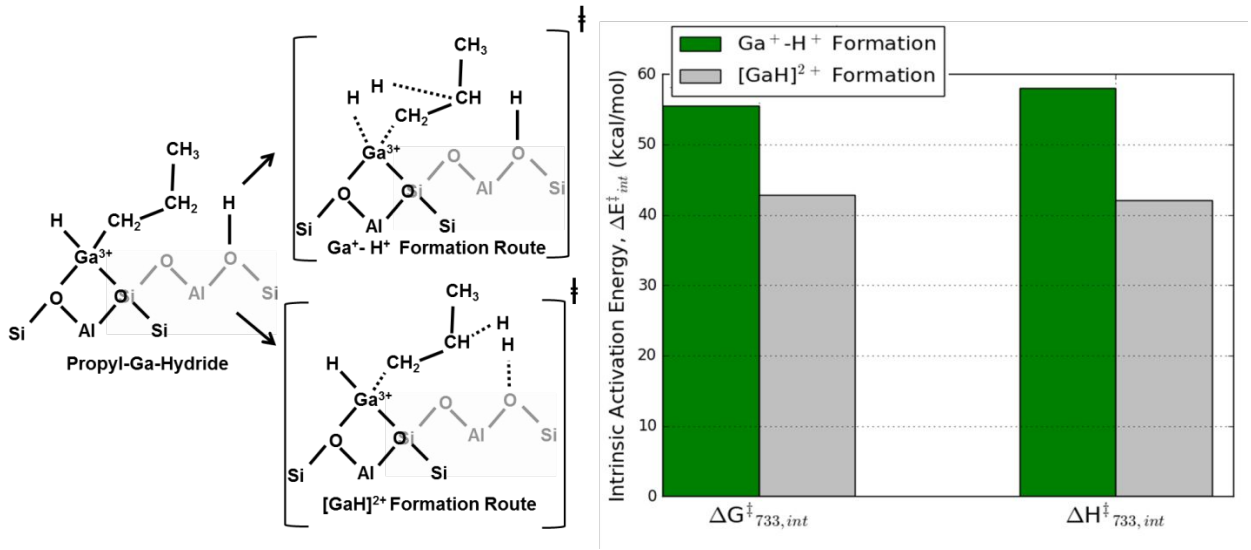

Figure S15. Free Energy and enthalpy barriers for C_3H_6 formation from C_3H_7-Ga-hydride intermediates, reported at 733 K, 10 kPa C_3H_8, 0.5 kPa C_3H_6, 0.5 kPa C_2H_4, and 0.5 kPa CH_4.

Text S.6 Estimation of exchange stoichiometries of Ga^{3+} species H_2-reduced Ga/H-MFI via NH_3-TPD and density of $[GaH]^{2+}$ cations in Ga/H-MFI samples

In a recently published study, our group developed protocols for the synthesis of well-defined and isolated Ga^{3+} cations in Ga/H-MFI via the vapor-phase exchange of dehydrated H-MFI with $GaCl_3$.[5] These materials were characterized using a number of spectroscopic and chemical probes in order to elucidate the structure of Ga^{3+} species under oxidizing and reducing conditions. These findings were also corroborated with the aid of theoretical calculations.

H_2 –temperature programmed reduction, infrared spectroscopy, Ga K-edge XANES (X-Ray Absorption Near Edge Spectroscopy) and EXAFS (Extended X-Ray Absorption Fine Structure) and theoretical calculations suggested at that at low Ga/Al ratios and under reducing anhydrous conditions, $[GaH]^{2+}$ and $[GaH_2]^{+}$-H^{+} cation pairs form in Ga/H-MFI.[5] The relative proportion of these cationic species can be determined on the basis of their exchange stoichiometry (H^{+} exchanged per Ga^{3+} atom) because $[GaH]^{2+}$ cations titrate 2 Brønsted acid O-H groups (H^{+}) per Ga^{3+} atom while $[GaH_2]^{+}$ cations titrate 1 Brønsted acid O-H group (H^{+}) per Ga^{3+} atom. The exchange stoichiometry of Ga/H-MFI samples was determined on the basis of titration of residual Brønsted acid O-H groups in Ga/H-MFI by NH_3. The quantity of NH_3 adsorbed was determined by means of NH_3 –temperature programmed desorption experiments.

These experiments were conducted over H_2-reduced Ga/H-MFI samples using protocols developed by Di Iorio et al. that enable the selective titration of residual Brønsted acid O-H groups in metal-exchanged zeolites, without concomitant titration of metal cations by NH_3.[6] The reader is referred to our characterization study of Ga/H-MFI for exact details of the experimental

procedures used here to conduct NH_3-TPD experiments over Ga/H-MFI.[5] We find that NH_3-TPD spectra conducted in this fashion show only a feature at 660 K representative of NH_3 desorption from Brønsted acid O-H groups.[5] The quantity of NH_3 desorbed can be estimated by integrating the area under this feature. An assumption of a 1:1 stoichiometry between NH_3 desorbed and H^+ leads to an estimate of the concentration of residual Brønsted acid O-H groups in the sample. This quantity together with the density of Brønsted acid O-H groups per Al_{tot} present in the parent in the H-MFI sample can be used to compute the fraction of Brønsted acid O-H groups replaced per Al_{tot} atom. When normalized by the Ga/Al ratio, the exchange stoichiometry – H^+ exchanged per Ga^{3+} atom is obtained. The exchange stoichiometries for H_2- reduced Ga/H-MFI samples are shown in Table S2. Since $[GaH]^{2+}$ cations are expected to possess an exchange stoichiometry of 2 H^+_{exch} per Ga^{3+} atom, the density of $[GaH]^{2+}$ /Al can be readily estimated, as shown in Table S1. This density is similar within error (H^+_{exch}/Ga estimates have errors of ± 20%) to the expected density of $[GaH]^{2+}$ if a 100% of Ga at a Ga/Al ratio of 0.1 is $[GaH]^{2+}$ and if further increases in Ga/Al ratio do not lead to the formation of any additional $[GaH]^{2+}$.

For the Ga/Al = 0.05 sample and 0.5 sample, errors in NH_3-TPD quantification were too large to accurately determine the density of $[GaH]^{2+}$ cations. On the basis of the trend observed in Table S2, where the fraction of $[GaH]^{2+}$ is maximum at a Ga/Al ratio of 0.1, it was assumed that the close distance (≤ 5 Å) proximate cation-exchange sites that have been found to be required for the formation of $[GaH]^{2+}$ cations in our previous work[5] would be saturated at a Ga/Al ratio of 0.1. For Ga/Al ratios less than 0.1 therefore, it was assumed that a sufficient concentration of such cation-exchange sites would be available for Ga^{3+} siting and therefore a 100% of the Ga would be present at $[GaH]^{2+}$ cations. This analysis leads to an estimate of 0.05 $[GaH]^{2+}$ /Al_{tot} for a Ga/Al ratio of 0.05. For the Ga/Al = 0.5 sample, it was assumed any

additional Ga exceeding a Ga/Al ratio of 0.1 in this sample would not form $[GaH]^{2+}$ cations.

Therefore, a value of 0.1 $[GaH]^{2+}/Al_{tot}$ was assumed for this sample.

Table S2: $H^{+}_{exch}/H^{+}_{total}$, H^{+}_{exch}/Ga and $[GaH]^{2+}/Al_{tot}$ values measured via NH_3-TPD after H_2 treatment of Ga/H-MFI samples at 823 K.

Ga/Al	H^{+}_{exch}/H^{+}_{tot}	H^{+}_{exch}/Ga[a]	Predicted H^{+}_{exch}/Ga[b]	$[GaH]^{2+}/Al_{tot}$
0.1	0.2	2.2	2.0	0.1
0.2	0.3	1.5	1.5	0.1
0.3	0.4	1.2	1.3	0.1

[a] Obtained from NH_3-TPD profiles of H_2-treated Ga/H-MFI samples. NH_3/Al_{tot} values from these experiments were used together with eq (2) in order to estimate H^{+}_{exch}/H^{+}_{tot}. These values were then normalized by the Ga/Al_f ratio (obtained by dividing Ga/Al_{tot} values by the Al_f/Al_{tot} value for H-MFI, to reflect framework Al_f in order to obtain values of H^{+}_{exch}/Ga)

[b] Predicted values are based on the assumption that 100% of Ga at a Ga/Al ratio of 0.1 is present as $[GaH]^{2+}$ cations and no further $[GaH]^{2+}$ is product upon further increases in Ga content

References:

(1) Biscardi, J. A.; Iglesia, E. Structure and Function of Metal Cations in Light Alkane Reactions Catalyzed by Modified H-ZSM5. *Catal. Today* **1996**, *31*, 207–231.

(2) Rodrigues, V. D. O.; Faro Júnior, A. C. On Catalyst Activation and Reaction Mechanisms in Propane Aromatization on Ga/HZSM5 Catalysts. *Appl. Catal. A Gen.* **2012**, *435–436*, 68–77.

(3) Vannice, Albert, M. *Kinetics of Catalytic Reactions*; Springer US: New York, 2005.

(4) Rooney, J. J. Eyring Transition-State Theory and Kinetics in Catalysis. *J. Mol. Catal. A Chem.* **1995**, *96*, L1–L3.

(5) Phadke, N.; Van der Mynsbrugge, J.; Mansoor, E.; Getsoian, A.; Head-gordon, M.; Bell, A. T. Characterization of Isolated Ga^{3+} Cations in Ga / H-MFI Prepared by Vapor-Phase Exchange of H-MFI Zeolite with $GaCl_3$. *ACS Catal.* **2018**, *8*, 6106–6126.

(6) Di Iorio, J. R.; Bates, S. A.; Verma, A. A.; Delgass, W. N.; Ribeiro, F. H.; Miller, J. T.; Gounder, R. The Dynamic Nature of Brønsted Acid Sites in Cu-Zeolites During NO_x Selective Catalytic Reduction: Quantification by Gas-Phase Ammonia Titration. *Top. Catal.* **2015**, *58*, 424–434.